Nanoscale

Accepted Manuscript

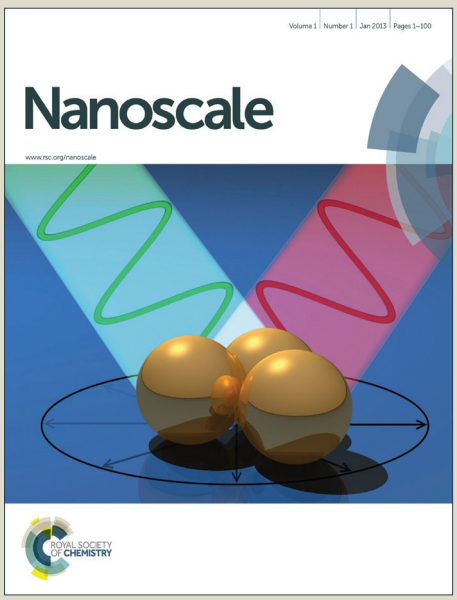

ROYAL SOCIETY OF CHEMISTRY

www.rsc.org/nanoscale

Nanoscale

ARTICLE

Nanoscale electric polarizability of ultrathin biolayers on insulator substrates by electrostatic force microscopy

Received 00th January 20xx,
Accepted 00th January 20xx

DOI: 10.1039/x0xx00000x

www.rsc.org/

A. Dols-Perez[a], G. Gramse[b], A. Calò[c], G. Gomila[d,e] and L. Fumagalli[f †]

We measured and quantified the local electric polarization properties of ultrathin (~ 5 nm) biolayers on mm-thick mica substrates. We achieved it by scanning a sharp conductive tip (< 10 nm radius) of an electrostatic force microscope over the biolayers and quantifying sub-picoNewton electric polarization forces with a sharp-tip model implemented using finite-element numerical calculations. We obtained relative dielectric constants ε_r = 3.3, 2.4 and 1.9 for bacteriorhodopsin, dioleoylphosphatidylcholine (DOPC) and cholesterol layers, chosen as representative of the main cell membrane components, with an error below 10% and a spatial resolution down to ~ 50 nm. The ability of using insulating substrates common in biophysics research, such as mica or glass, instead of metallic substrates, offers both a general platform to determine the dielectric properties of biolayers and a wider compatibility with other characterization techniques, such as optical microscopy. This opens up new possibilities for biolayer research at the nanoscale, including nanoscale label-free composition mapping.

Introduction

The electric polarization properties of ultrathin biological layers made of proteins, lipids or sterols in response to an external electric field play an important role in many areas of science and technology. In particular, they are inherently coupled to cell membrane bioelectric phenomena in excitable and non-excitable cells such as membrane potential formation, action potential propagation or ion membrane transport[1-4]. Moreover, they largely determine the cell response to externally applied electrical fields in electrokinetic techniques such as dielectrophoresis,[5] impedance spectroscopy[6] or electroporation.[7] Finally, they are key in many electrical and electrochemical biosensors, in particular capacitive and impedance biosensors, which base their electro-transducing mechanism on changes in the dielectric properties of integrated biolayers upon sensing[8,9]. Therefore, determining the electric polarization properties of biolayers, commonly represented by the dielectric constant, ε_r, is of great importance. However, their ultrathin thickness (~ 5 nm) and extremely soft and fragile nature make dielectric constant quantification a challenging task. To this aim, specific measurement techniques have been developed in the past to access this important physical property, such as electrical impedance spectroscopy of cell suspensions[10-12], capacitance patch-clamp of single cells and micrometric membrane patches[13,14] and impedance spectroscopy of planar lipid bilayers either deposited on electrodes[15,16] or suspended on apertures separating two compartments[17]. But the spatial resolution of these techniques is in the microscale range (in the best of the cases) and hence they cannot resolve the ultrastructure of biolayers, where rich biochemical and bioelectrical phenomena take place.

In recent years, a number of scanning probe microscopy (SPM) techniques sensitive to the nanoscale electrical polarization properties of materials has been developed. Techniques such as nanoscale capacitance microscopy[18-20], electrostatic force microscopy[21-28], nanoscale impedance microscopy[29,30], scanning polarization force microscopy[31-34], scanning microwave microscopy[35,36] or nanoscale non-linear dielectric microscopy[37], have progressively increased the spatial resolution of dielectric measurements in general, and in particular applied to ultrathin biolayers[20-22]. Dielectric SPM techniques are well suited to the study of soft biolayers because they offer the advantage of gentle imaging conditions and of an extremely high spatial resolution down to the nanoscale range, which is not achievable by standard characterization techniques. So far, however, accurate measurements of the local dielectric properties of ultrathin biolayers have only been reported for biolayers on metallic substrates such as gold and graphite or on highly-doped silicon substrates[20-22]. These substrates are used as bottom electrode of a standard two-electrode measurement setup, with the nano-sized tip of the SPM system being used as top electrode. This configuration guarantees high signal

[a.] Institut de Química Avançada de Catalunya (IQAC-CSIC), C/ Jordi Girona 18 – 26, 08034, Barcelona (Spain). CIBER of Bioengineering, Biomaterials and Nanomedicine (CIBER-BBN), Barcelona, Spain.
[b.] Johannes Kepler University Linz, Institute for Biophysics, Gruberst. 40, 4020-Linz, Austria.
[c.] CIC NanoGUNE Consolider, E-20018 Donostia San Sebastian, Spain.
[d.] Nanobioelec group, Institut de Bioenginyeria de Catalunya (IBEC), Baldiri i Reixac 15-21, 08028-Barcelona, Spain.
[e.] Departament d'Electrònica, Universitat de Barcelona, C/ Martí i Franquès 1, 08028 Barcelona, Spain
[f.] School of Physics and Astronomy, University of Manchester, Oxford Road, Manchester, M13 9PL, United Kingdom.
† Corresponding author: laura.fumagalli@manchester.ac.uk
Electronic Supplementary Information (ESI) available: modelling sharp probes on insulator substrates, probe geometry calibration.

noise ratio and simple theoretical modelling of the system. But it severely limits the variety of biolayers that can be studied, because biolayers typically do not adsorb easily to metallic substrates, unless specific immobilization strategies are used, e.g. sulphur-tagged molecules for binding on gold substrates or gold substrate oxidation, which make the meaurement more complicated and less accurate.

Here, we overcome this limitation and show that nanoscale dielectric properties of ultrathin biolayers can be accurately measured on top of mm-thick insulating substrates such as mica or glass conventionally used in biolayer research[38]. These substrates have very flat surfaces and almost all biolayers tend to spontaneously adsorb to them without requiring any special treatment, thus making this approach of wide applicability. Dielectric SPM techniques have already been applied to insulating substrates[39-41], but the possibility of quantifying the dielectric properties of ultrathin film biolayers of only few-nm thickness and sub-micrometre width deposited on them has still to be demonstrated. In particular, existing dielectric images of liquid islands and self-assembled monolayers on insulators obtained with scanning polarization force microscopy[31-34] or of biomolecules and nanoparticles on mica obtained with electrostatic force microscopy[42,43] are still awaiting quantitative interpretation. We achieved it here by combining a number of advances, namely, by taking *low-noise* electrostatic force microscopy images using soft cantilevers, thus achieving the sub-picoNewton force resolution required to probe such ultrathin layers on a thick insulator; by taking EFM images in *constant-height* mode with accurate scan-height control, thus avoiding topographic artefacts and tip-substrate distance uncertainty that would impede dielectric quantification; by carefully implementing a *two-step calibration* procedure based on force-distance curves to obtain the geometric parameters of the micrometric probe (tip radius, cone angles and cantilever width) that play a role on thick insulators; by fitting the EFM images to a theoretical model that accurately reproduces the complex electrostatic interaction of the whole microscopic probe over ultrathin layers on top of thick insulators; finally, by using wear-resistant doped-silicon probes instead of standard metal-coated probes. Metal-coated probes were appositely avoided in this work because structurally unstable due to tip wear. They would make it extremely difficult to achieve dielectric constant quantification with the accuracy required here. We remark that in order to use doped-silicon probes, which show a sharpened tip apex with respect to metal-coated probes, here we implemented an advanced model with a *double-cone* geometry that reproduces both the short-range electrostatic interaction of the sharpened cone and the long-range effects that contribute on thick insulator substrates[44,45], in contrast with the simple case of metallic substrates where only the short-range contribution of the end of the single-cone tip plays a role[27]. The developed methodology has been successfully applied here to determine the local dielectric constant of three ultrathin biolayer samples, bacteriorhodopsin, dioleoylphosphatidylcholine (DOPC) and cholesterol, representative of the three main components of natural biomembranes, namely, proteins, lipids and sterols. By using the sharpest commercially available probes for this type of measurements (doped-silicon probes with tip radius of ~ 5 nm), we show here that high spatial resolution is achieved, while keeping high precision in dielectric constant, that is, better than 10% precision sub-micrometric wide patches, with the potential of reaching 20% precision on extremely small patches down to only 20 nm in diameter.

Results

The dielectric constant of the biolayer patches deposited on the insulator substrate is obtained from ultra low-noise images of the local capacitance gradient (~ 0.1 zF/nm resolution, sub-picoNewton forces) using amplitude modulated electrostatic force microscopy in constant-height mode (Fig. 1).

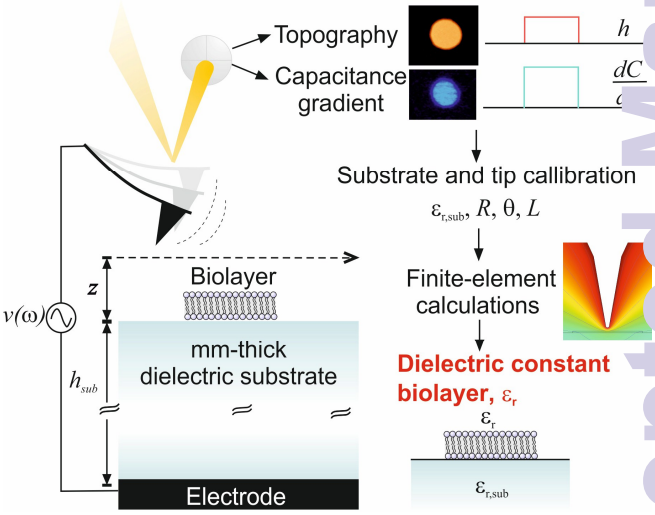

Figure 1. Schematic representation of the setup and data analysis procedure used to determine the dielectric constant of the ultrathin biolayers on the insulator substrate.

The experimental data are matched to a sharp tip-biolayer model which includes long-range cantilever contributions (Fig. 2a) solved with finite-element numerical calculations (see details in the Experimental section). The tip geometry is obtained by applying a specific two-step calibration procedure and the biolayer geometry/size is obtained from standard topography imaging, so that the dielectric constant of the biolayer patch is the *only* fitting parameter of the analysis procedure. An example of electric potential distribution at two magnification levels is shown in Fig. 2b and 2c.

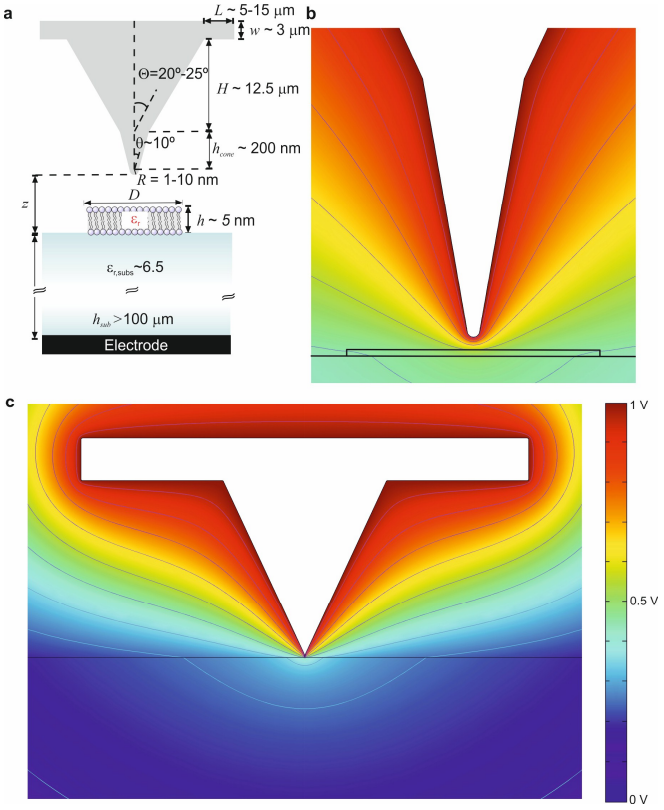

Figure 2. (a) Schematic representation of the sharp tip-biolayer model implemented with finite-element numerical calculations (not to scale). A dual-angle cone model that mimics the short-range effects given by the sharpened silicon tip geometry is used. A large disc is included to take into account the long-range effects of the cantilever. The values of parameter that determine probe geometry/size are obtained from a specific double step calibration procedure. (b) Calculated electrostatic potential distribution around the probe apex and (c) the overall calculated probe corresponding to the interaction of the probe with a biolayer patch on an insulating substrate. Parameters used in the calculations: L = 10 μm, H = 12.5 μm, w = 2 μm, Θ = 25º, θ = 10º, h_{cone} = 200 nm, R = 5 nm, h = 5 nm, D = 200 nm, ε_r = 2 and z = 15 nm.

As representative examples of biolayers, we have chosen biolayers made of three of the main components of natural membranes (proteins, lipids and sterols), specifically bacteriorhodopsin, 1,2-Dioleoyl-sn-glycero-3-phosphocholine (DOPC) and cholesterol. Bacteriorhodopsin is one of the prototypical membrane proteins and it has been widely studied[46]. It acts as proton pump in some Archaea, and naturally forms 2D crystalline membranes of ~ 5 nm thickness, with the presence of only a very small amount of lipids (typically in a 1:10 ratio (mol:mol)). Once formed, bacteriorhodopsin membranes can be easily deposited on planar substrates and remain stable under dry conditions. DOPC is a widely used representative example of unsaturated phospholipids and phosphocholines, which constitute the more abundant phospholipids in eukaryotic cells[47]. DOPC single bilayers are ~ 5 nm thick and they can be formed on flat freshly-cleaved mica substrates under dry conditions by spin-coating as shown in Ref. 48. By using this procedure the lipid bilayers show a remarkable stability as well as structural and mechanical properties very similar to their analogues prepared in aqueous solutions[48].

Cholesterol is an important component of eukaryotic cell membranes, especially in mammals, being the major non-polar lipid of cell membranes[49]. It is responsible of 20% of the membra weight and has a major role in processes such as endocytocis an exocytosis. It also plays an important role in modulating physic properties of the cell membranes such as membrane orderin[50] permeability[51] and stiffness[52,53] , and it is involved in the membran dynamic clustering, i.e. the formation of lipid rafts[54-56]. Due to the rigid ring structure of cholesterol molecules, and to the poor balanc between their hydrophilic and hydrophobic parts, monocomponent samples of cholesterol tend to form platelike crystals containing or or multiple cholesterol bilayers with thickness multiple of ~ 3.7 nm[57,58].

Figure 3a shows the topography obtained of a single-layer bacteriorhodopsin patch on mica, with diameter ~ 1.5 μm and thickness h ~ 5.3 nm (see also the topographic profile in Fig. 3c). Fi 3b gives the dielectric image (dC/dz) recorded at the scan height z_0 ~ 18 nm.

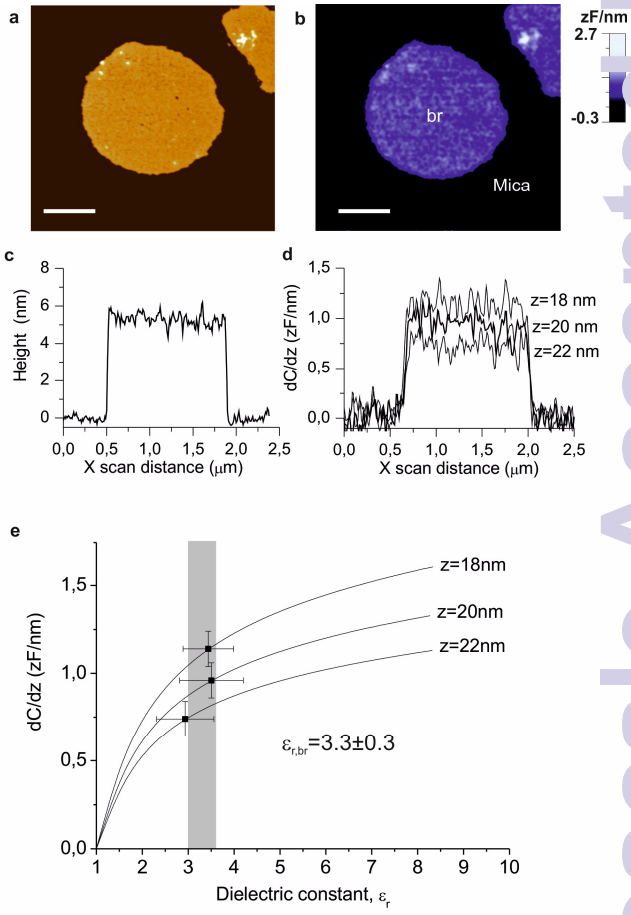

Figure 3. Dielectric constant measurement of the bacteriorhodopsin single layer patch on an insulator substrate. (a) Topography of a bacteriorhodopsi monolayer patch on a mica substrate. (b) Dielectric image taken at a *constant-height* z_0 = 18 nm from the substrate. Scale bar: 500 nm. The radius of the t was previously calibrated on a metal substrate, giving R = 5.5 nm, θ = 7.4º. The cantilever disc radius was calibrated on the mica surface giving L = 13 μm (with $\varepsilon_{r,sub}$ ~ 6.5). In the tip calibration we fixed h_{cone}= 400 nm, H = 12.5 μ

= 2 μm and Θ = 25º. (c) Topography and (d) dielectric profiles at different heights taken across the center of the patch, showing the typical height of ~ 5.3 nm and a dielectric signal around 1zF/nm decreasing with distance. (e) Calculated capacitance gradient constrast, *dC/dz*, (lines) as a function of the ε_r of the biolayer patch using the measured parameters (z_0, *D*, *h*, *R*, θ, *L*), with $\varepsilon_{r,br}$ as the *only* fitting parameter. By matching the average signal measured on the patch (symbols) for each height, we obtained an average value of $\varepsilon_{r,br}$ ~ 3.3 ± 0.3. The error bars in (e) are given by the detection noise of 0.1 zF/nm, while the color-shaded region show the standard deviation of the measurement.

The calibrated probe radius was *R* = 5.5 ± 0.25 nm and the sharpened cone half-angle θ = 7.4 ± 0.3º (obtained on metal) and *L* = 13.0±0.5 μm (obtained on the bare mica substrate). To calibrate the tip geometry, we fixed h_{cone} = 400 nm, *H* = 12.5 μm, *w* = 2 μm and Θ = 25º. The dielectric image shows a clear dielectric signal contrast corresponding to the ultrathin small patch, although it only amounts ~ 1 zF/nm (see dielectric profiles in Fig. 3d), thus demonstrating the high sensitivity of EFM (~ 0.1 zF/nm noise level). We repeated the measurement at three different scan heights (z_0 = 18, 20, 22 nm, see profiles in Fig. 3d) and fitted the dielectric data to finite-element simulations. Fig. 3e shows the calculated capacitance-gradient contrast (lines) and measured contrast (symbols) as a function of the dielectric constant, showing that the obtained dielectric constant is $\varepsilon_{r,br}$ ~ 3.3 ± 0.3.

These results demonstrate that the dielectric constant of small biolayer patches can be obtained on insulating substrates with EFM, despite the challenges imposed by these substrates in both measurement and quantification respect to the case of using metallic substrates. In particular, the precision with which the dielectric constant value is obtained (~ 10% relative error) is remarkable, considering the effect of the insulating substrates (reduction in signal by a factor around 4 as compared to the use of metallic substrates) and of using very small silicon tips (additional reduction in signal by a factor 4 as compared to typical metal-coated tips).

In Fig. 4a we show a large scale topographic image of the DOPC lipid single bilayer patches. They show a thickness of ~ 5 nm and a diameter between microns and few hundreds of nanometers. We[48], and others[59], have shown earlier that the bilayer patches sit on a lipid monolayer ~1.3 nm thick, as schematically shown in Fig. 4b. The presence of this monolayer can be shown to be negligible in the quantification procedure used here because it only modifies the dielectric constant of the substrate to a very small extent due to its small thickness and polarizability (less than a 1% in agreement with the predictions of Ref. 60). A dielectric image obtained on a single lipid bilayer patch around 700 nm wide is shown in Fig. 4d together with the corresponding topographic image in Fig. 4c. Images taken at different tip-substrate distance reveal the corresponding variation of the capacitance gradient contrast as a function of tip substrate distance (see Fig. 4f). By using the calibrated tip parameters (*R* = 2.8 ± 0.25 nm, θ = 11 ± 0.3º, *L* = 7.0 ± 0.5 μm) and the sample topography (*h* = 5 nm, *D* = 700 nm), the fitting of the finite-element numerical calculations gives a dielectric constant value of $\varepsilon_{r,DOPC}$ ~ 1.9 ± 0.2.

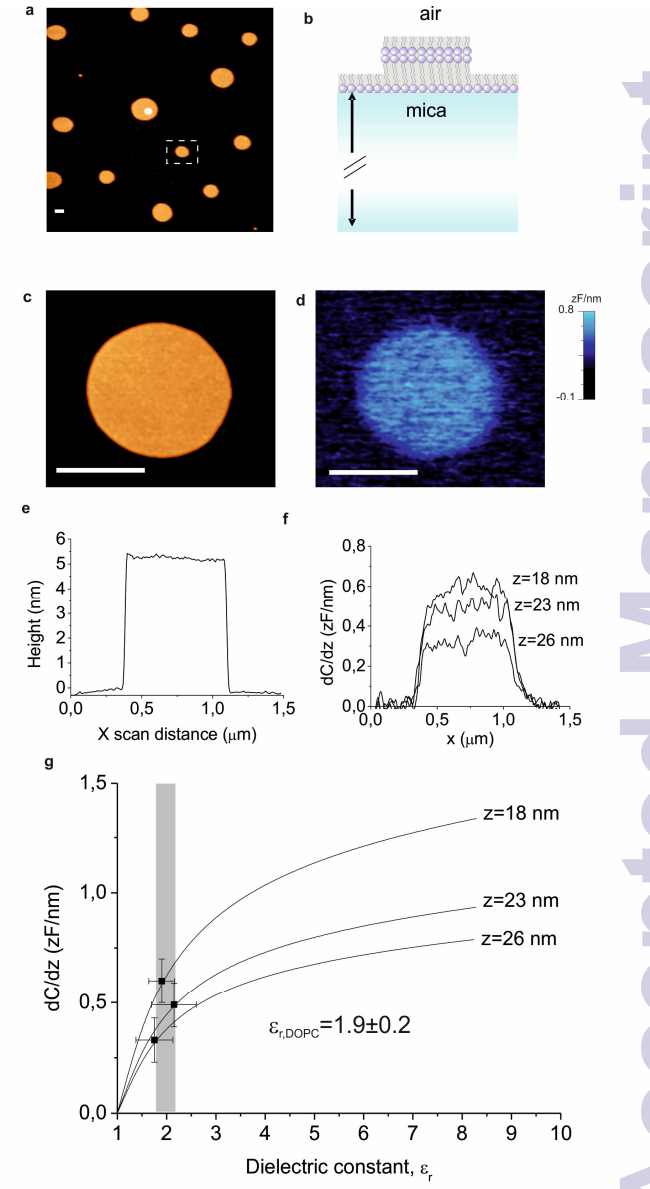

Figure 4. Dielectric constant measurement of a DOPC bilayer patch on an insulator substrate. (a) Large scale image of the topography of DOPC bilayer patches of different diameters on a mica substrate. (b) Schematic representation of the structure of the DOPC bilayer patches. (c) Topographic image and (d) dielectric image taken at *constant-height* at z_0 = 18 nm from the substrate taken on a single bilayer patch of diameter *D* = 700 nm. Scale bar: 500 nm. The radius of the tip was previously calibrated on a metal substrate, giving *R* = 2.8 nm and θ = 11.2º. The cantilever disc radius was calibrated on the mica surface giving *L* = 7 μm (with $\varepsilon_{r,}$ ~ 6.5). In the tip calibration we fixed *h*=400 nm, *H*=12.5 μm, *w*=2 μm and Θ=24 (e) Topography and (f), dielectric profiles taken across the center of the patch showing the typical height of ~ 5 nm and dielectric signal decreasing with distance. (g) Calculated capacitance gradient contrast, *dC/dz*, (lines) as a function of the ε_r of the lipid bilayer using the measured parameters (*z*, *D*, *R*, θ, *L*) and $\varepsilon_{r,DOPC}$ as the only fitting parameter. By matching the average signal measured on the patch (symbols) for each height, we obtained an average value of $\varepsilon_{r,DOPC}$ ~ 1.9 ± 0.2. The error bars in (g) are given by the detection noise of 0.1 zF/nm while the colour-coded region shows the standard deviation of the measurement.

Finally, Fig. 5 shows the cholesterol sample topography, dielectric image and corresponding profiles, together with the fitting of the numerical calculations to the measured dielectric contrasts

different heights. The final result obtained from the quantification procedure, where we approximated the size and shape of the cholesterol crystal by a disc of ~ 7 nm thickness and lateral dimension approximately equal to the width of the crystal, D ~ 1μm, gives a dielectric constant of $\varepsilon_{r,chol}$~2.3 ± 0.1. This value is slightly higher than the value obtained for the DOPC patches and slightly smaller than the one obtained for bacteriorhodopsin patches, indicating an intermediate dielectric polarizability of the cholesterol crystals as compared to the other biomembrane components.

Discussion

We have shown that the dielectric constant of ultrathin small scale biolayer patches can be quantified on insulating substrates with a high precision (relative error below a 10%) and unparalleled lateral resolution. We have demonstrated it by measuring the dielectric constant of DOPC lipid bilayer patches ($\varepsilon_{r,DOPC}$~ 1.9 ± 0.2), which is remarkably close to the value obtained for bulk oils and hydrocarbons ($\varepsilon_{r,oils}$~ 2.1)[61] and close to the value normally associated to the hydrophobic core of lipid bilayers ($\varepsilon_{r,lipids}$ ~ 2.1)[62]. This validates the technique and shows its high accuracy (around 10%) in addition to the increased lateral resolution achieved with respect to standard techniques, as we discuss further below. The accuracy of the technique is confirmed by the measurements on Purple Membrane patches. The dielectric constant that we obtained here ($\varepsilon_{r,br}$ ~ 3.2 ± 0.3) matches (with accuracy below 10%) the value obtained in bulk on very low hydrated samples using standard dielectric spectroscopy ($\varepsilon_{r,PM}$ ~ 3.3 at 1 MHz and 21% water content[63]).

We emphasise that the dielectric constant reported here for lipid bilayers (~ 2) is the first direct measurement at the single bilayer level on a *dry* sample. In hydrated samples a slightly larger value is expected due to hydration effects, as we previously reported for another lipid bilayer dipalmitoylglycerophosphocholine (DPPC) ($\varepsilon_{r,DPPC}$~ 3.3)[22]. We remark that the dielectric constant of ~ 3 that we measured here for dried bacteriorhodopsin proteins, which compose the Purple Membrane, matches the value that we recently obtained using EFM on conductive substrates on the dried proteins that compose the T7 bacteriophage capsid[28] ($\varepsilon_{r,protein}$ = 3.5 ± 0.5 for the shell and tail proteins). It is also in remarkable agreement with the value ~ 3.5 measured on dried protein powders at bulk level[64] and with the generally recognized value for dried proteins ~ 2.5-3.5, slightly larger than the dielectric constant of lipids, which was verified by theoretical calculations[65]. In particular, the remarkably close values around ~ 3 measured on different dried proteins confirm the theoretical prediction of small dependence of dielectric constant on protein structure and composition and it reflects the low-polarizable hydrophobic core of proteins. We note that we previously reported slightly smaller values for Purple Membrane patches on metallic substrates with nanoscale capacitance microscopy ($\varepsilon_{r,PM}$~ 1.9 ± 0.2)[20] and *static* EFM ($\varepsilon_{r,PM}$~ 1.78 ± 0.07)[21], which we attribute to both the higher resolution/accuracy of the measurement setup and the more accurate theoretical modelling implemented in our recent works[27,28,66] with respect to our early estimations[20,21].

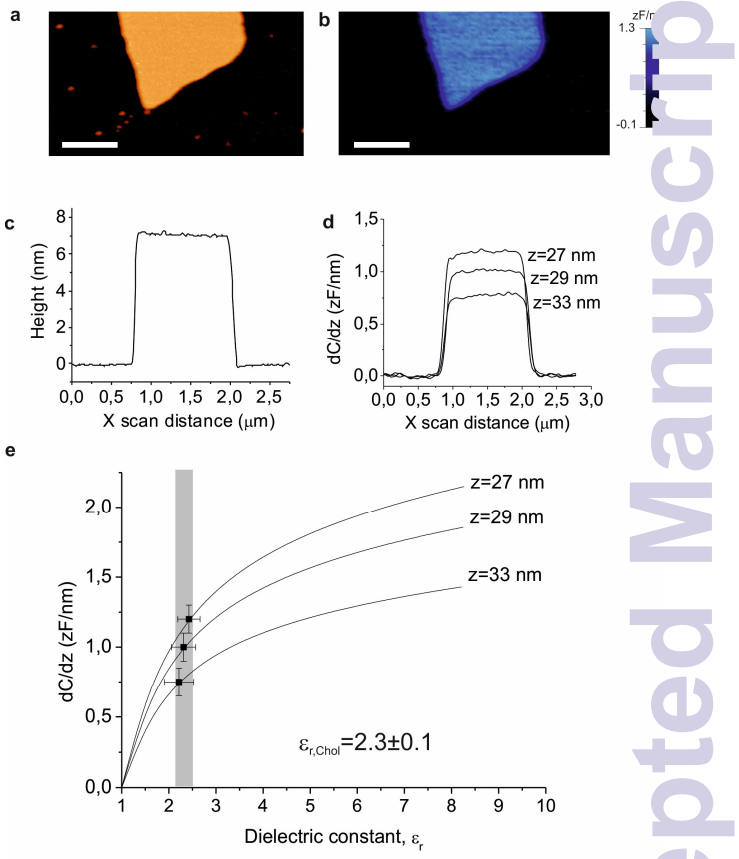

Figure 5. Dielectric constant measurement of a Cholesterol layer patch on an insulator substrate. (a) Topography of the Cholesterol layer on a mica substrate. (b) Dielectric image taken at *constant-height* at z_0 = 27 nm from the substrate. Scale bar: 500 nm. The radius of the tip was previously calibrated on a metal substrate, giving R = 19.5 nm, θ = 2.6º. The cantilever disc radius was calibrated on the mica surface close to the biolayer patch, giving L = 27 μm (with $\varepsilon_{r,subs}$ ~ 6.5). In the tip calibration we fixed h = 400 nm, H = 12.5 μm, w = 2 μm and Θ = 15º. (c) Topography and (d), dielectric profiles taken across the center of the patch, showing a height of ~ 7 nm and a dielectric signal decreasing with z distance. (e) Calculated capacitance-gradient contrast, dC/dz, (lines) as a function of the ε_r of the cholesterol crystal using the measured parameters (z, D, R, θ, L) and $\varepsilon_{r,Chol}$ as the *only* fitting parameter. By matching the average signal measured on the layer (symbols) for each measuring height, we obtained an average value of $\varepsilon_{r,Chol}$ ~ 2.3 ± 0.1. The error bar in (e) is given by the detection noise of 0.1 zF/nm while the colour-coded region shows the standard deviation of the measurements.

Concerning the dielectric constant of cholesterol crystals that we obtained here ($\varepsilon_{r,chol}$ ~ 2.3 ± 0.1), to our knowledge this is the first direct measurement reported either at the nanoscale or on bulk samples, thus showing the versatility and potential of our technique. So far only indirect information on the dielectric properties of cholesterol have been reported, which were obtained from macroscopic impedance spectroscopy measurements on egg phosphatidylcholine bilayers mixed with cholesterol (at 2:1 molar ratio). These measurements revealed only a marginal variation in the specific capacitance of the bilayer upon addition of cholesterol, from c_{eggPC} ~ 0.61 μF/cm² to $c_{eggPC+chol}$ ~ 0.7 μF/cm²,[67], which is consistent

with the fact demonstrated here that cholesterol has a dielectric constant only slightly larger than that of lipid bilayers.

The values obtained for the three biolayers measured here lie in the range ~ 2-3, with slight differences between the constituents (the larger value corresponds to the protein layer and the smallest one to the lipids, with cholesterol lying in between). This result indicates that despite the highly heterogeneous composition of natural biomembranes, their dielectric response should be relatively homogeneous, showing only slight variation between different biochemical components.

The consistency of the results reported here with existing results at larger scale (when available) and the high accuracy and precision (~ 10%) with which we obtained them at the highest spatial resolution definitively supports the wide applicability of EFM for quantification of dielectric properties of ultrathin biolayer patches on top of mm-thick insulating substrates.

Finally here below we discuss the minimum biolayer patch size that can be *detected and quantified* and the expected spatial resolution of our technique. Figure 6 shows the evolution of the capacitance-gradient contrast (left axis) and of the relative error in the extracted dielectric constant (right axis) as a function of the patch diameter for a membrane patch of dielectric constant $\varepsilon_r = 2$ and thickness $h = 5$ nm interacting with a characteristic sharp tip ($R = 5$ nm, $\theta = 10º$, $\Theta = 25º$, $h = 200$ nm, $H = 12.5$ μm and $L = 10$ μm). Results are shown for an insulating substrate with $\varepsilon_{r,subs} = 6.5$ (blue symbols) and for a metallic substrate (red symbols). In all cases the tip-substrate measuring distance has been kept to $z_0 = 15$ nm. The relative error has been calculated as

$$\frac{\delta\varepsilon_r}{\varepsilon_r} = \frac{\delta\Delta C'_{inst}}{\varepsilon_r \frac{\partial}{\partial\varepsilon_r}\Delta C'(z,\varepsilon_r,D)} \quad (1)$$

where, $\delta\Delta C'_{inst}$ is the instrumental noise, assumed to be 0.1 zF/nm (which constitutes a good trade-off between different practical experimental constraints). The contrast is seen to be approximately constant for diameters $D > 100$ nm (it is not exactly constant as it shows a very smooth variation) and starts to decrease sharply for diameters $D < 100$ nm. By setting the detection limit of the instrument to ~ 0.1 zF/nm the smallest detectable patch is around ~ 9 nm in diameter for the case of an insulating substrate and around ~ 4 nm for the metallic substrate. Therefore, despite the fact that the signal on insulating substrates is significantly lower than on metal substrates (around a factor 4 in the present case), the use of insulating substrates does not severely limit the size of the smallest detectable patch as compared to the use of metallic substrates. In parallel to the reduction in the signal when the size of the membrane patch is reduced, the relative error of the quantified dielectric constant increases. In the case of insulating substrates the error goes below 20% for membrane patch diameters just above 20 nm (and below 10% for patch diameters above 100 nm). In the case of metallic substrates the situation is slightly better due to the higher signal-to-noise ratio - the relative error goes below 20% already for patch diameters of only 6 nm (and below 10% for patch diameters larger than 10 nm). In any case, this demonstrates that the dielectric quantification of biolayer patches on insulating substrates can be achieved with high precision down to nearly biomolecular sizes.

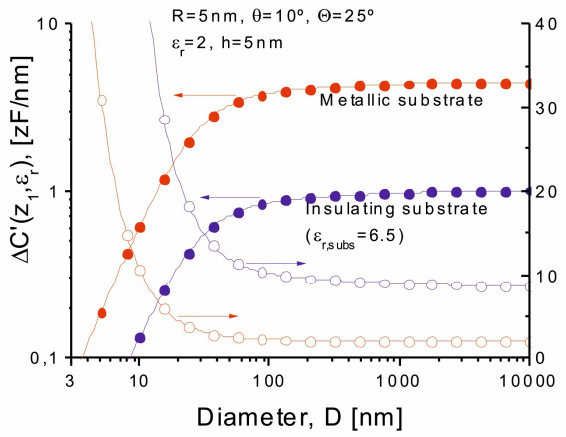

Figure 6. (Left axis, solid symbols) Capacitance-gradient contrast as a function of the diameter of the biolayer patch (dielectric constant $\varepsilon_r = 2$ and thickness $h = 5$ nm) on an insulating substrate ($\varepsilon_{r,sub} = 6.5$) (blue symbols) and on a metallic substrate (red symbols) calculated for a characteristic sharpened tip ($R = 5$ nm, $\theta = 10º$, $\Theta = 25º$, $h = 200$ nm, $H = 12.5$ μm and $L = 10$ μm). The tip-substrate distance is set to 15 nm. (Right Axis, empty symbols) Relative error in the extracted dielectric constant as a function of the diameter for the same system for an instrumental noise of 0.1 zF/nm.

The spatial resolution of the measurements is also remarkable. We have experimentally evaluated it by determining the distance at which the measured capacitance gradient contrast profiles decrease to half its maximum value. For the PM profiles shown in Fig. 3c we obtained $\Delta x_{res,diel}$ = 50 ± 5 nm, 60 ± 5 nm and 70 ± 5 nm for the measuring distances of z_0 = 18 nm, 20 nm and 22 nm, respectively. Within the relatively large uncertainty of these estimations, the spatial resolution seems to follow a linear increase with tip sample-distance with a slope ~ 5 nm/nm. This latter result is compatible with the theoretical calculations reported in Ref. 68, where it is predicted that on insulator substrates the spatial resolution increases linearly with tip-substrate distance in the whole range of measuring distances. The extrapolation of the obtained results allows predicting a spatial resolution of $\Delta x_{res,diel}$ ~ 10 nm at the closest practical measuring distance of z_0~ 10 nm. This spatial resolution is comparable to the topographic spatial resolution, $\Delta x_{res,topo}$~ 10 nm / 2 nm obtained from the topographic profile in Fig. 3b. This demonstrates that the spatial resolution achievable with sharpened probes on insulating substrates is near to the molecular size for both topographic and dielectric imaging.

We note that for physiological studies it would be necessary to perform the dielectric measurements in liquid environment. At present, the extension of EFM to the liquid environment has only

been achieved for metallic substrates[69-71], including the study of lipid DPPC bilayer patches[22]. However, from the theory of EFM measurements in liquid media[72] it is not immediate that they can be easily extended to insulating substrates, since innovative solutions would be required to achieve that.

Finally, we mention a potential interesting application of the results obtained here, i.e. the label-free mapping of the composition of hetereogeneous membranes through the measurement of the local dielectric constant. With the results reported here, although the main biomembrane components do not seem to show large differences in their dielectric constants, their difference is enough to be detectable, at least for medium size domains of the order of 100 nm. Indeed, from Fig. 3e, for instance, one can estimate a change in contrast of ~ 0.3 zF/nm for a measuring distance of z_0 = 18 nm when passing from a region rich in lipids (ε_r ~ 2) to a region rich in proteins (ε_r ~ 3). Although it is a small change, it should be detectable with present instrumentation due to the impressive precision with which quantification can be achieved (sensitivity below ~ 0.1 zF/nm).

Experimental

Nanoscale dielectric measurements. We performed dynamic electrostatic force microscopy (EFM) measurements with a commercial atomic force microscope (AFM) (Nanotec Electronica S.L) operated in dry air conditions (1% humidity) and room temperature. Dynamic EFM was implemented in amplitude modulation, meaning that we applied an alternating voltage of amplitude v_{ac} and angular frequency ω between the conductive tip and the bottom of the insulating substrate in order to excite the mechanical oscillation of the cantilever. We detected the induced oscillation in the deflection at 2ω, using a lock-in amplifier, while scanning the tip over the dielectric sample deposited on the mm-thick insulating substrate (Fig. 1). Differently from standard amplitude-modulation AFM (AM-AFM), in which the amplitude is used as feedback signal to obtain the topography, here the amplitude of oscillation is acquired at 2ω to directly obtain the capacitive (electrostatic) interaction, related to the dielectric properties of the sample, through the expression $F_{2\omega}(x,y,z) = C_z'(x,y,z)\cdot v_{ac}^2/4$, where $C_z'(x,y,z)$ is the probe-sample capacitance gradient in the *z*-direction, which depends on the probe-sample geometry and the dielectric constant of the biolayer and substrate. In order to maximise the signal-to-noise ratio of the measurement, we used soft cantilevers (PPP-CONTR, Nanosensors) with spring constant of 0.2-0.5 N/m and resonance frequency 15-20 kHz. By driving the cantilever with a frequency of oscillation of 1 kHz, well below the mechanical resonance of the cantilever, we obtained the capacitive interaction directly from the deflection amplitude at 2ω (2kHz), $D_{2\omega}(x,y,z)$, as $C_z'(x,y,z) = D_{2\omega}(x,y,z)\ 4k/v_{ac}^2$, where *k* is the cantilever spring constant. We used the measured values of spring constant provided by the manufacturer after verifying that they are equal to the values obtained by thermal noise measurement within 10% error. We also verified that the dielectric constants reported here do not depend on the cantilever spring constant, similarly as we previously demonstrated in Ref. 27 for the case of measurement on conductive substrates.

In order to quantify the dielectric constant, we measured the 2ω signal *at constant height* with respect to the substrate. This means that the feedback is switched off at the beginning of each line, so that the tip always remains at the same distance (height) *z* from the insulating substrate while scanning, independently of the location over the biolayer or on the bare substrate - as sketched in Figure 1. and no mechanical oscillation is applied to the probe. This enables us to avoid topographic cross-talks into the dielectric image, as it happens in SPFM, which uses the 2ω-signal as feedback control signal, or in other techniques that use constant tip-sample distance (the so called *lift-mode*) so that the obtained dielectric properties are modulated by the topography of the sample and their quantification is more complicated. By using constant-height mode, the dielectric contrast directly reflects the variation of electric polarization of the layer with respect to the air surrounding it, that is the dielectric constant, and not the variation of the tip distance/height. To avoid direct stray contributions from micrometric parts of the probe (the cantilever and the upper part of the cone), we calculated the capacitance gradient *contrast,* $\Delta C'(x,y,z,\varepsilon_r) = C'(x,y,z,\varepsilon_r) - C'(x_0,y_0,z,\varepsilon_r)$, where (x_0, y_0) is a reference position on the bare substrate. By analyzing $\Delta C'(x,y,z,\varepsilon_r)$ rather than the absolute value $C'(x,y,z,\varepsilon_r)$, we directly obtain the *local* dielectric image. We precisely measured the scan height, *z,* with respect to the dielectric substrate and precisely determined it (Δz = ± 0.5 nm) by recording both the deflection and the capacitance gradient as a function of the tip-substrate distance at the image edges. The dc deflection provides the distance from the substrate, while the capacitance gradient was used to determine and compensate any vertical piezo drift (typically 2-3 nm) by comparison with the tip calibration fit curve. All the data were taken applying 5V, scan speed 1 sec per line, achieving ~ 0.05 zF/nm electrical resolution corresponding to a force of ~ 0.3 pN.

We used highly-doped silicon tips with nominal radius < 7 nm, which we preferred to metal-coated silicon tips because they exhibit smaller tip radius and show minimum radius variation during the experiments. We found that the radius of silicon tips remained constant within ± 0.25 nm during the set of measurements required for dielectric constant extraction. We carefully checked it by repeating the probe geometry calibration before and after each experiment.

Quantification of the membrane local dielectric constant. To quantify the dielectric constant of the biolayer patches, ε_r, we used finite-element numerical calculations (COMSOL MULTIPHYSICS 4.3, AC/DC electrostatic module) to solve for Poisson's equation and calculate the force acting on the tip, because an accurate analytical model including the microscopic effects of the cone and cantilever on insulator substrates is not available. We performed 2D axial symmetric simulations using the Pardiso solver and the specific probe model developed for the sharp silicon probes in Ref. 73. This model takes into account the particular shape of sharp silicon tips,

with a cone half-angle of 15º-25º that tapers to a smaller angle around 10º at the very end of the tip. To this end, we modelled the probe with a dual-angle cone model, which consists of a microscopic truncated cone of height *H* and cone half-angle Θ ended with a sharpened smaller truncated cone of height h_{cone} and half-angle θ ended with a semi-spherical apex of radius, *R* (Fig. 2a). Note that contrary to some situations in metallic substrates[27,73], the explicit use of the full dual-angle cone model is necessary on insulator substrates, due to relevance of indirect effects that depend on the microscopic parts of the probe (see Supplementary Information). We also included in the model a disc on top of the cone to account for the *effective* effects of the cantilever, as we described in Ref. 45 for the case of single angle tip models. The disc has a radius $R_{disc} = L + H\tan(\Theta)$ and thickness *w*, where *L* (that we will refer to as cantilever radius) is the part of the disc cantilever overseeing the cone base. The biolayer patch is modelled as a disc of relative dielectric constant, ε_r, diameter, *D*, and thickness *h* directly obtained from the width and height of the topographic image. No geometric parameter related to the substrate thickness is used because we modelled it as semi-infinite, as we previously demonstrated that results do not depend on the substrate thickness, provided this is larger than ~ 100 μm,[41]. On the other hand, the dielectric constant of the mica substrate is taken to be $\varepsilon_{r,subs}$ = 6.5, as we showed earlier using a similar approach[41,45]. The full model used is schematically shown in Fig. 2a, while in Fig. 2b,c we show an example of an electric potential distribution at two different levels of magnification. The global meshing used is extra fine with boundary mesh-size < 100 nm on the probe and < R/ 5 on the smaller cone of the tip (apex). The electrostatic force is obtained from the calculations by using the built-in Maxwell stress function, from where the capacitance gradient is obtained as for the experimental measurements. We evaluated the accuracy of the calculations against the analytical formula of the electrostatic force of a sphere on an infinite dielectric and found it better than 1%. The quantification of the dielectric constant of the biolayer patches, ε_r, is obtained by fitting the measured capacitance gradient contrast values to the predictions of the finite element numerical simulations, calculated with the geometric values obtained from the calibrated probe geometry (see below) and the measured sample topography[27]. In this procedure, the dielectric constant of the biolayer is the single fitting parameter of the model. The dielectric constants obtained within the present framework are representative of the average dielectric properties of the biolayers on the lateral scale achieved here (roughly ~ 50 nm lateral resolution).

Probe geometry calibration. In the analysis we have kept the microscopic cone geometry, the cantilever thickness and the apex cone height fixed to a nominal value within the range given by the manufacturer (*H* = 12-15 μm, Θ = 15º-25º, *w* = 2-3 μm, h_{cone} = 0.2-0.4 μm), and fitted the tip radius, *R*, the cantilever radius, *L*, and the half-angle of the sharpened cone end, θ, by using a *two step calibration procedure.* First, the tip radius was calibrated by fitting a short range force-distance curve taken over a metallic substrate while keeping the sharp cone angle fixed to its nominal value θ = 10º (*tip calibration*). Then, the value of the cone angle, θ, is refined by fitting a longer range force-distance curve on a metallic substrate by keeping the radius *R* fixed to the value determined from the sh[illegible] range curve. Finally, with the same tip, a second force-distance curv[illegible] on the dielectric substrate – over which the sample is deposited - [illegible] used to set the *effective* value of the cantilever radius, *L*, so that [illegible] local dielectric constant of the insulator substrate, $\varepsilon_{r,subs}$, (= 6.5 fo[illegible] mica) is precisely obtained (*disc calibration*). This elaborated calibration procedure is the adaptation of the procedure develope[illegible] for single-cone probes on insulator substrates and of dual-angle con[illegible] probes on metallic substrates for nanoparticle characterization (Ref[illegible] 45 and 73, respectively). Calibration curves are shown in th[illegible] Supplementary Information.

Samples and sample preparation. Here, bacteriorhodopsi[illegible] membranes were prepared from a lyophilized powder of purple membrane from *Halobacterium salinarum* (Sigma Aldrich). Th[illegible] powder was resuspended in high purity MilliQ water (Millipore) to a final concentration of 0.5 mg/ml, deposited on a flat freshly-cleaved mica sheet and incubated for ~ 20 min at room temperature, a[illegible] which it was gently dried out into a nitrogen flow prior to its use. DOPC single bilayers on mica were prepared following the s[illegible] coating method detailed in Ref. 48. In the present case we used DOPC hexane solution of a concentration 0.25 mM. Finally cholesterol ultrathin layers were prepared on mica also by the spi[illegible] coating technique. Solutions of cholesterol (Sigma Aldrich) wer[illegible] prepared in pure hexane (Sigma Aldrich) at the concentration of 0.25-0.5 mM. A volume of about 100 µL was spinned onto freshl[illegible] cleaved mica (velocity: 3000 rpm, acceleration: 4000 rpm/s, time: 1 minute), and the sample was stored for 24 h in dark and in low vacuum conditions (0.1 mbar) to remove all solvent residuals. In these conditions lath shaped cholesterol crystals ~ 7 nm thick wer[illegible] easily and reproducibly formed on the mica surface. AFM measurements on all samples were performed in dry conditions (R[illegible] ~ 1%, under nitrogen flow).

Conclusions

We have demonstrated the ability of amplitude modulate[illegible] electrostatic force microscopy to measure the local dielectric constant of ultrathin biolayer patches (~ 5nm thick) on mm[illegible] thick insulator substrates with a non-invasive procedure, goo[illegible] precision and nanoscale spatial resolution. Given the simplicit[illegible] of biolayer preparation on this type of substrates, presen[illegible] results open the possibility to study local electric polarizatio[illegible] properties of a large variety of ultrathin biolayers. We showe[illegible] that the use of mm-thick insulator substrates has practically no cost in terms of spatial resolution and minimum latera[illegible] dimensions of the detectable biolayers with respect to the use of metallic substrates. Furthermore it offers a broade[illegible] compatibility with other microscopy techniques such as optical techniques by enabling to use glass substrates. The nanoscale spatial resolution of the technique allows accessing the local dielectric properties of biolayers - not averaged over large areas as in macroscopic techniques. It also provides high accur[illegible]

because it has access to the precise geometry/size of the biolayer (thickness and diameter) *in-situ*, which is not possible using macroscopic techniques. The proposed method could help in obtaining an accurate map of the dielectric properties of heterogeneous biolayers i.e. natural cell membranes, thus improving present theoretical models of nanoscale bioelectric phenomena such as membrane electroporation or ion membrane transport, and could represent one of the first label-free composition mapping techniques for biolayer research.

Acknowledgements

This work was supported by the Spanish MINECO under grants TEC2010-16844 and TEC2013-48344-C2. (GG) acknowledges support from an ICREA Academia grant from the Generalitat de Catalunya. We acknowledge useful discussion with Dr. M. A. Edwards.

References

1 J. Malmivuo, J. R. Plonsey, Bioelectromagnetism: principles and applications of bioelectric and biomagnetic fields; Oxford University Press: New York, 1995.
2 J. A. Dilger, S. G. A. McLaughlin, T. J. McIntosh, and S. A. Simon, *Science*, 1979, **206**, 1196.
3 A. Warshel, P. K. Sharma, M. Kato, and W. W. Parson, *Biochim. Biophys. Acta*, 2006, **1764**, 1647.
4 H. G. L. Coster, *J. Biol. Phys.*, 2003, **29**, 363.
5 H. A. Pohl, *Dielectrophoresis: the behaviour of neutral matter in nonuniform electric fields*; Cambridge University Press: London, 1978.
6 S. Grimnes, O. Martinsen, *Bioimpedance and bioelectricity basics*; Academic Press: San Diego, 2000.
7 J. C. Weaver, and Y. A. Chizmadzhev, *Bioelectrochem. Bioenerg.*, 1996, **41**, 135.
8 Ch. Berggren, and B. Bjarnason, G. Johansson, *Electroanal.* 2001, **13**, 173.
9 J. S. Daniels, and N. Pourmand, *Electroanal*., 2007, 12, 1239.
10 R. Lisin, B.-Z. Ginzburg, M. Schlesinger, and Y. Feldman, *Biochim. Biophys. Acta*, 1996, **1280**, 34.
11 Y. Polevaya, I. Ermolina, M. Schlesinger, B.-Z. Ginzburg, and Y. Feldman, *Biochim. Biophys. Acta-Biomem.*, 1999, **1419**, 257.
12 K. Asami, *J. Non-Cryst. Solids*, 2002, **305**, 268.
13 M. Lindau, and E. Neher, *Pflugers Arch.*, 1988, **411**, 137.
14 L. J. Gentet, G. J. Stuart and J. D. Clements, *Biophys. J.*, 2000, **79**, 314.
15 C. Steinem, A. Janshoff, W-P. Ulrich, M. Sieber, and H.-J. Galla, *Bioch. Biophys. Acta*, 1996, **1279**, 169.
16 G. L. H. Coster, T. C. Chilcott, and A. C. F. Coster, *Bioelectrochem. Bioenerg.*, 1996, **40**, 79.
17 R. Benz, O. Frohlich, P. Lauger, and M. Montal., *Biochim. Biophys. Acta.*, 1995, **394**, 323.
18 D. T. Lee, J. P. Pelz and B. Bhushan, *Nanotechnology*, 2006, **17**, 1484.
19 L. Fumagalli, G. Ferrari, M. Sampietro, and G. Gomila, *Appl. Phys. Lett.*, 2007, **91**, 243110.
20 L. Fumagalli, G. Ferrari, M. Sampietro, and G. Gomila, *Nano Lett.*, 2009, **9**, 1604.
21 G. Gramse, I. Casuso, J. Toset, L. Fumagalli, and G. Gomila *Nanotechnology*, 2009, **20**, 395702.
22 G. Gramse, A. Dols-Pérez, M. A. Edwards, L. Fumagalli, and G. Gomila, *Biophys. J.*, 2013, **104**, 1257.
23 W. Lu, D. Wang, and L. W. Chen, *Nano Lett.*, 2007, **7**, 2729.
24 C. Riedel, R. Arinero, Ph. Tordjeman, M. Ramonda, G. Lévêque, G. A. Schwartz, D. Garcia de Oteyza, A. Alegria, and J. Colmenero, *J. Appl. Phys.*, 2009, **106**, 024315.
25 C. Riedel, R. Arinero, Ph. Tordjeman, G. Lévêque, G. A. Schwartz, A. Alegria, and J. Colmenero, *Phys. Rev. E*, 2010, **81**, 010801.
26 O. Cherniavskaya, L. Chen, L. Weng, L. Yuditsky, and L.-E. Brus *J. Phys. Chem. B*, 2003, **107**, 1525.
27 L. Fumagalli, D. Esteban-Ferrer, A. Cuervo, J. L. Carrascosa and G. Gomila, *Nat. Mat.*, 2012, **11**, 808.
28 A. Cuervo, P. D. Dans, J. L. Carrascosa, M. Orozco, G. Gomila and L. Fumagalli, *PNAS*, 2014, **111**, E3624.
29 R. Shao, S. V. Kalinin, and D. A. Bonnell, *Appl. Phys. Lett.*, 2003, **82**, 1869.
30 L. S. C. Pingree, and M. C. Hersam, *Appl. Phys. Lett.*, 2005, **87**, 233117.
31 J. Hu, X. Xiao, and M. Salmeron, *Appl. Phys. Lett.*, 1995, **67**, 476.
32 J. Hu, X. D. Xiao, D. F. Ogletree, and M. Salmeron, *Science* 1995, **268**, 267.
33 A. Verdaguer, M. Cardellach, and J. Fraxedas, *J. Chem. Phys.*, 2008, **129**, 174705.
34 J. J. Benitez, O. Rodriguez de la Fuente, I. Díez-Pérez, F. Sanz, and M. Salmeron, *J. Chem. Phys.*, 2005, **123**, 104706.
35 K. Lai, M. B. Ji, N. Leindecker, M. A. Kelly, Z.-X. Shen, *Rev. Sci. Instrum.*, 2007, **78**, 063702.
36 K. Lai, W. Kundhikanjana, M. A. Kelly, S.-X. Shen, *Appl. Nanosci.*, 2011, **1**, 13.
37 Y. J. Cho, *J. Mat. Research.*, 2011, **26**, 2007.
38 V. J. Morris, A. R. Kirby, A. P. Gunning, *Atomic Force Microscopy for Biologists*; Imperial College Press:London, 1999.
39 C. Gao, T. Wei, F. Duewer, Y. Lu, and X.-D. Xiang, *Appl. Phys. Lett.*, 1997, **71**, 1872.
40 K. Lai, W. Kundhikanjana, M. A. Kelly, and Z. X. Shen, *Appl. Phys. Lett.*, 2008, **93**, 123105.
41 L. Fumagalli, G. Gramse, D. Esteban-Ferrer, M. A. Edwards, and G. Gomila, *Appl. Phys. Lett.*, 2010, **96**, 183107.
42 A. Takagi, F. Yamada, T. Matsumoto and T. Kawai, *Nanotechnology*, 2009, **20**, 365501.
43 E. Mikamo-Satoh, F. Yamada, A. Takagi, T. Matsumoto and T. Kawai, *Nanotechnology*, 2009, **20**, 145012.
44 G. M. Sacha and J. J. Sáenz, Appl. Phys. Lett., 2004, 85, 2610.
45 G. Gramse, G. Gomila and L. Fumagalli, *Nanotechnology*, 2012, **23**, 205703.
46 U. Haupts, J. Tittor, D. Oesterhelt, *Ann. Rev. Biophys. Biomol. Struct.*, 1999, **28**, 367.
47 G. Meer, D. R. Voelker, and G. W. Feigenson, *Nat. Rev. Mol. Cell Biol.*, 2008, **9**, 112.
48 A. Dols-Perez, L. Fumagalli, A. C. Simonsen, G. Gomila *Langmuir*, 2011, **27**, 13165.
49 B. Alberts, A. Johnson, J. Lewis, M. Raff, K. Roberts and P. Walter, *Molecular Biology of the cell*, 4th edition, Garland Science:New York, 2002.
50 S. Bhattacharya and S. Haldar, *Biochim. Biophys. Acta*, 2000, **1467**, 39-53.
51 S. Raffy and J. Teissié, *Biophys. J.*, 1999, **76**, 4, 2072.
52 F. J. Byfield, H. Aranda-Espinoza, V. G. Romanenko, G. H. Rothblat and I. Levitan, *Biphys. J.*, 2004, **87**, 3336.
53 R. Serral-Gracià, N. Bezlyepkina, R. L. Knorr, R. Lipowsky and R. Dimova, *Soft Matter*, 2010, **6**, 1472.
54 K. Simons, E. Ikonen, *Nature*, 1997, **387**, 569.
55 D. Lingwood, K. Simons, *Science*, 2010, **327**, 46.
56 D. A. Brown, E. London, *Annu. Rev. Cell Dev. Biol.*, 1998, **14**, 111.
57 H. S. Shieh, L. G. Hoard, C. E. Nordman, *Nature*, 1977, **267**, 287.
58 B. M. Craven, *Nature*, 1976, **260**, 727.

59 M. Hirtz, R. Corso, S. Sekula-Neuner, and H. Fuchs, *Langmuir*, 2011, **27**, 11605.
60 E. Castellano-Hernández and G. M. Sacha, *Appl. Phys. Lett.*, 2012, **100**, 023101.
61 A. D. Sent, V. G. Anicich and T. Arakelian *J. Phys. D Appl. Phys.* 1992, **25**, 516
62 R. Pethig, D. B. Kell, *Phys. Med. Biol.*,1987, **32**, 933.A.
63 Buchsteiner, R. E. Lechner, T. Hauss, N. A. Dencher, *J. Mol. Biol.*, 2007, **371**, 914.
64 S. Takashima, H. P. Schwan, *J. Phys. Chem.,* 1965, **69**, 4176
65 M. K. Gilson, B. H. Honig, Biopolymers, 1986, **25**, 2097
66 G. Gomila, G. Gramse, L. Fumagalli, *Nanotechnology*, 2014, **25**, 255702.
67 R. G. Ashcroft, H. G. L. Coster, D. R. Laver, J. R. Smith, *Bioch. Biophys. Acta Biomem.*, 1983, **730**, 231.
68 C. Riedel, A. Alegría, G. A. Schwartz, J. Colmenero and J. J. Sáenz, *Nanotechnology*, 2011, **22**, 285705.
69 Y. Hirata, F. Mizutani, and H. Yokoyama, *Surf. Interface Anal.*, 1999, **27**, 317.
70 N. Kobayashi, H. Asakawa, and T. Fukuma, *Rev. Sci. Instrum.*, 2010, **81**, 123705.
71 G. Gramse, M. A. Edwards, L. Fumagalli, and G. Gomila, *Appl. Phys. Lett.*, 2012, **101**, 213108.
72 G. Gramse, M. A. Edwards, L. Fumagalli, and G. Gomila, *Nanotechnology*, 2013, **24**, 415709.
73 L. Fumagalli, M. A. Edwards and G. Gomila, *Nanotechnology*, 2014, **25**, 495701.